NRC Publications Archive
Archives des publications du CNRC

Cracking phenomena in In(0.25)Ga(0.75)AS films on InP substrates
Wu, X.; Weatherly, G. C.

This publication could be one of several versions: author's original, accepted manuscript or the publisher's version. / La version de cette publication peut être l'une des suivantes : la version prépublication de l'auteur, la version acceptée du manuscrit ou la version de l'éditeur.
For the publisher's version, please access the DOI link below./ Pour consulter la version de l'éditeur, utilisez le lien DOI ci-dessous.

Publisher's version / Version de l'éditeur:
https://doi.org/10.1016/S1359-6454(99)00211-6
Acta Materialia, 47, 12, pp. 3383-3394, 1999-09-29

NRC Publications Record / Notice d'Archives des publications de CNRC:
https://nrc-publications.canada.ca/eng/view/object/?id=4a3e57b6-0160-41c0-beae-b1c4d1b230b8
https://publications-cnrc.canada.ca/fra/voir/objet/?id=4a3e57b6-0160-41c0-beae-b1c4d1b230b8

Access and use of this website and the material on it are subject to the Terms and Conditions set forth at
https://nrc-publications.canada.ca/eng/copyright
READ THESE TERMS AND CONDITIONS CAREFULLY BEFORE USING THIS WEBSITE.

L'accès à ce site Web et l'utilisation de son contenu sont assujettis aux conditions présentées dans le site
https://publications-cnrc.canada.ca/fra/droits
LISEZ CES CONDITIONS ATTENTIVEMENT AVANT D'UTILISER CE SITE WEB.

Questions? Contact the NRC Publications Archive team at
PublicationsArchive-ArchivesPublications@nrc-cnrc.gc.ca. If you wish to email the authors directly, please see the first page of the publication for their contact information.

Vous avez des questions? Nous pouvons vous aider. Pour communiquer directement avec un auteur, consultez la première page de la revue dans laquelle son article a été publié afin de trouver ses coordonnées. Si vous n'arrivez pas à les repérer, communiquez avec nous à PublicationsArchive-ArchivesPublications@nrc-cnrc.gc.ca.

National Research Council Canada
Conseil national de recherches Canada

Canada

PERGAMON

Acta mater. Vol. 47, No. 12, pp. 3383–3394, 1999
© 1999 Acta Metallurgica Inc.
Published by Elsevier Science Ltd. All rights reserved.
Printed in Great Britain
1359-6454/99 $20.00 + 0.00

PII: S1359-6454(99)00211-6

CRACKING PHENOMENA IN $IN_{0.25}Ga_{0.75}AS$ FILMS ON InP SUBSTRATES

X. WU and G. C. WEATHERLY†

Department of Materials Science and Engineering, McMaster University, Hamilton, Ontario, Canada L8S 4L7

(Received 9 February 1999; accepted 6 July 1999)

Abstract—The strain relaxation of a series of $In_{0.25}Ga_{0.75}As$ films grown on (100) InP substrates (lattice mismatch = 2%) has been studied by electron microscopy. The mechanisms of strain relief (in the first stages of growth) occurred by cracking on $(0\bar{1}1)$, and by twinning on (111) and $(\bar{1}11)$ planes. Cracking was a transitory process with the density of cracks being highest in a 20 nm thick film, while a 500 nm thick film was crack-free. These results are discussed in the context of different cracking and crack-healing models. © *1999 Acta Metallurgica Inc. Published by Elsevier Science Ltd. All rights reserved.*

Keywords: Compound semiconductors; Fracture; Analytical electron microscopy

1. INTRODUCTION

The growth of highly perfect, planar, strained epitaxial films offers a number of interesting materials processing challenges in semiconductor device fabrication. One of the problems encountered in the growth of lattice-mismatched materials of high structural quality is strain relaxation. The most extensively studied strain relaxation mechanism is plastic flow—the development of dislocations along the substrate–film interface and the formation of microtwins [1–4]. Recently, a purely elastic strain relaxation mechanism has been demonstrated, both theoretically and experimentally—the strain energy stored in the film can be relaxed by creating surface instabilities [5–7]. A third strain relief mechanism in tensile strained layers is cracking. Although strain relaxation by cracking was first reported in 1972 [8], very few studies have been carried out on the cracking mechanism. Only recently has cracking in III–V epilayers attracted more attention due to the increasing technological interest in growing highly strained structures [9–11].

Matthews and Klokholm [8] first obtained the critical thickness (h_c) for the formation of a crack as $h_c = \gamma(1-\nu)^2/\pi\mu(1+\nu)f^2$ (γ is the surface energy, μ is the shear modulus, ν is Poisson's ratio and f is the misfit), using the Griffith criterion. This prediction agreed well with the experimental results of yttrium iron garnet films grown on rare earth–gallium or aluminium garnet substrates [12]. Murray *et al.* [10] studied crack formation in $In_x(GaAl)_{1-x}As$ epilayers grown under tension on InP (001) substrates. They proposed a simple theoretical model based on an energy balance criterion to predict the critical layer thickness for crack initiation, finding that $h_c = \gamma(1-\nu)/\mu(1+\nu)f^2$. This result was subsequently used by Dieguez *et al.* [11], who studied strain relaxation in the tensile $In_xGa_{1-x}As$/InP (001) system.

The fracture of films has also been widely studied, both theoretically and experimentally, in the context of cracking induced by thermal mismatch strains [13–16]. The film is assumed to be unconstrained as deposited, but a biaxial stress develops in the plane of the film on cooling. There is often a marked difference in the elastic constants of the film and substrate, and this can play an important role in the fracture behaviour [15–17]. However, the elastic constants of the film and substrate are usually very similar in III–V compound deposition. Another important distinction lies in the dynamic behaviour of cracking and crack-healing in the III–V compound situation, which probably occurs during film growth rather than on cooling to ambient temperature after growth.

In this paper, we report on a study of the cracking mechanisms in III–V heteroepitaxial strained layers. Two per cent tensile strained $In_{0.25}Ga_{0.75}As$ layers with thicknesses of 10, 20, 100, 200 and 500 nm grown on (100) InP substrates were chosen for this study. The results are analysed using models first developed to describe cracking associated with strain induced by a thermal mismatch [13–17].

2. EXPERIMENTAL PROCEDURE

Lattice-mismatched $In_{0.25}Ga_{0.75}As$ layers with a 2% tensile strain were grown on an *n*-type (100)

†To whom all correspondence should be addressed.

InP substrate at 480°C using gas-source molecular beam epitaxy (MBE) [7]. [011] and [0$\bar{1}$1] cross-sections and (100) plan-view transmission electron microscopy (TEM) samples were prepared following standard procedures and examined in a Philips CM12 operating at 120 kV and a JEOL 2010F field emission source TEM operating at 200 kV. Scanning electron microscopy (SEM) observations were conducted with a Philips 515 operating at 20 kV.

3. RESULTS

Figure 1(a) is a [011] cross-section TEM image of a 20 nm thick sample taken with $\mathbf{g} = 0\bar{2}2$. V-shaped cracks are visible. These cracks apparently nucleated at the edge or surface of the strained layer and penetrated into the substrate along the [100] growth direction. A TEM image of the same area taken with $\mathbf{g} = 200$ clearly shows that the strain relaxation by cracking is not homogeneous [Fig. 1(b)]. In this image the band of dark contrast in the substrate is a measure of the residual strains in the epilayer. The origin of this contrast, which arises because of surface relaxation of the stresses in the epilayer during TEM sample preparation, is discussed by Perovic *et al.* [18]. Only the strain at the crack tips has been relaxed while the areas between the crack tips are still strained. Figure 1(c) is a HRTEM image of a V-shaped crack, lying on the vertical (0$\bar{1}$1) plane in the strained layer. This crack has propagated about 10 nm into the substrate, before deviating on to an inclined {111} plane and finally terminating at a sharp tip. A close inspection of the lattice image of Fig. 1(c) shows terminating lattice-fringes near the crack tip, suggesting that there has been dislocation activity accompanying the final stage of crack propagation. This was confirmed by plan-view images. A (100) plan-view TEM image of the 20 nm thick layer sample (Fig. 2) revealed dislocations emanating from the crack tips.

The TEM image of the [0$\bar{1}$1] cross-section for the same layer (Fig. 3) shows a totally different structure from that observed in the [011] cross-section. Instead of cracks, an array of planar defects (microtwins or stacking faults) was observed in this cross-section.

The density of cracking as growth proceeded was followed by both SEM and XTEM. In the SEM

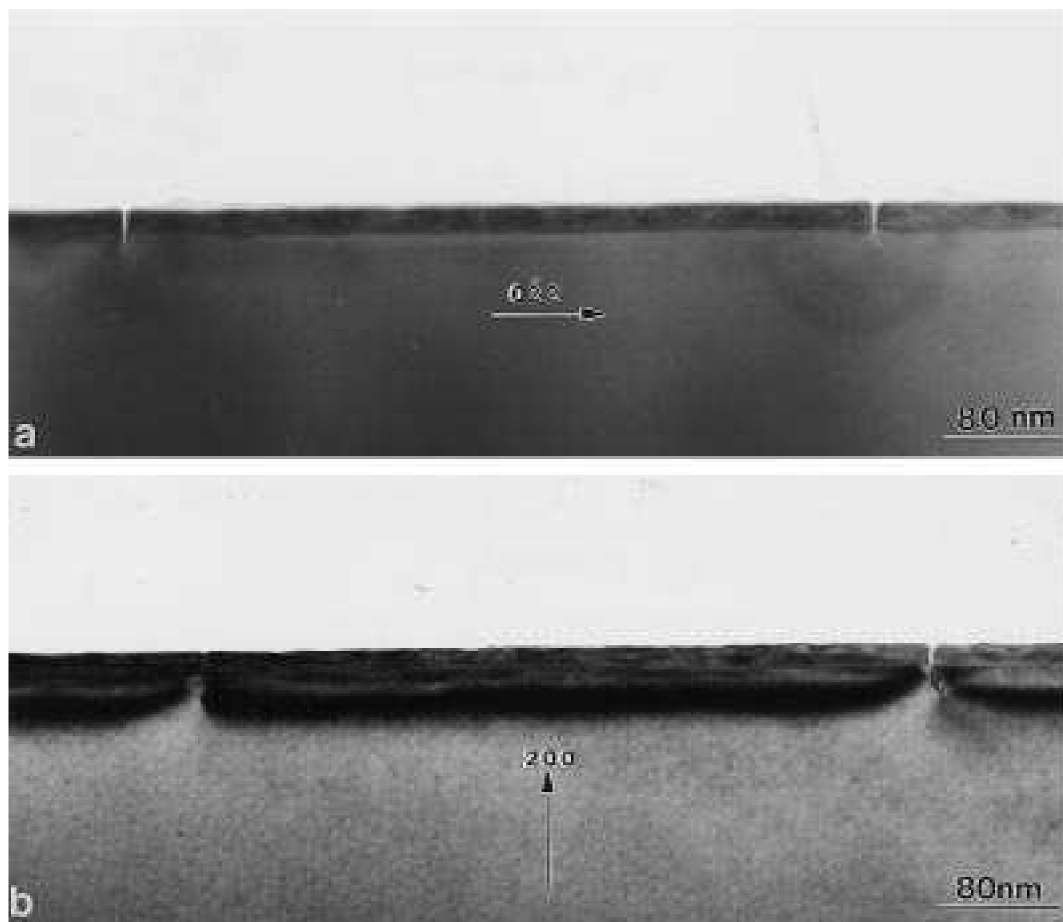

Fig. 1(a) and (b).

Fig. 1. Cracks in [011] cross-section of 20 nm layer sample. (a) $\mathbf{g} = 0\bar{2}2$ image showing V-shaped cracks. (b) $\mathbf{g} = 200$ image showing that the strain was relaxed at the tips of cracks but the areas between the crack tips are still strained. (c) HRTEM image of a crack showing that the crack deviates from the {011} plane on to the {111} plane after penetrating a distance of 10–15 nm into the substrate.

images (Fig. 4), the lines running along the [011] direction are the contrast from cracks, while the contrast along the $[0\bar{1}1]$ direction comes from surface roughness. [The crack opening displacement of the cracks (in the 20 nm thick film) lies below the resolution of the SEM (~5 nm). The cracks must be seen by topographic contrast, as the surface is slightly relaxed next to the cracks [10].] The SEM observations revealed that the crack spacing increases with an increase in layer thickness. No cracks were observed in the 10 and 500 nm thick samples (note that the 10 nm thick sample is not shown in Fig. 4). The TEM observations (Fig. 5) confirmed the SEM results: the crack spacing increases with an increase in layer thickness and no cracks were observed in either 10 or 500 nm thick layer samples. Table 1 summarizes the SEM and TEM observations of the crack dimensions with film thickness. The total crack length (c) and crack opening displacement (δ_0) are defined in Fig. 6, a STEM image from the 100 nm thick sample. This figure also displays part of an energy dispersive X-ray (EDX) analysis of the crack region (marked by an arrow in the figure). This is discussed in Section 4.4.

4. DISCUSSION

There are several interesting experimental observations which warrant further scrutiny: the critical thickness at which cracks nucleate (~20 nm in this study); a crack density that decreases as film growth proceeds beyond the critical thickness; the disappearance of cracks in the thickest film (500 nm); the anisotropy of cracking, and the penetration of cracks into the substrate, accompanied by the deviation of the crack plane from {011} to {111}.

Table 2 summarizes some of the relevant properties of the III–V compounds, which are used in the discussion that follows. The properties of

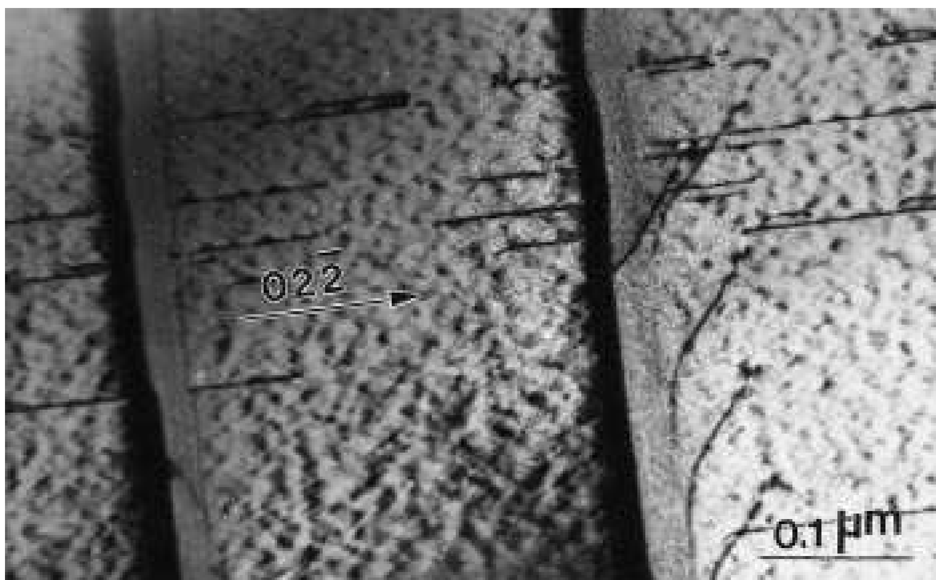

Fig. 2. (100) plan-view image with $\mathbf{g} = 02\bar{2}$ of 20 nm layer sample showing dislocations emanating from the crack tips. The dark–light contrast associated with the cracks is caused by surface strain relaxation effects.

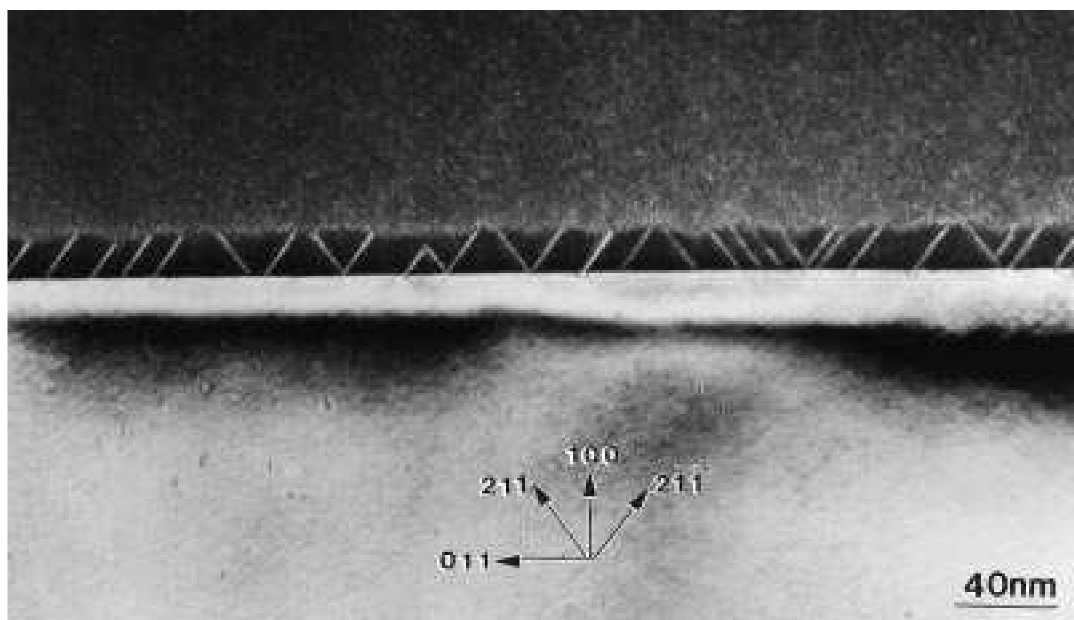

Fig. 3. $\mathbf{g} = 200$ dark field image showing planar defects (twins and stacking faults) in $[0\bar{1}1]$ cross-section of 20 nm layer sample.

$In_{0.25}Ga_{0.75}As$ have been estimated from data for InAs and GaAs, assuming Vegard's law behaviour. As noted in Section 1, the elastic properties of the film and substrate are similar. The two Dundurs parameters [19], α and β, are –0.103 and –0.003, respectively. Since these are both ≈ 0 the effect of elastic mismatch can be ignored. The thermal mismatch strain on cooling from the growth temperature to room temperature, 6×10^{-4}, is very much smaller than the growth strains, 2×10^{-2}, so this effect too can be safely ignored. Finally the estimated room temperature values of the surface energy of InP and $In_{0.25}Ga_{0.75}As$ are very similar, so the fracture resistance of the film and substrate are probably of the same order of magnitude (see Table 2).†

†Note that the value of γ has only been measured for GaAs. The values for the other compounds were estimated from the trends calculated by Cahn and Hanneman for all the Group III–V compounds.

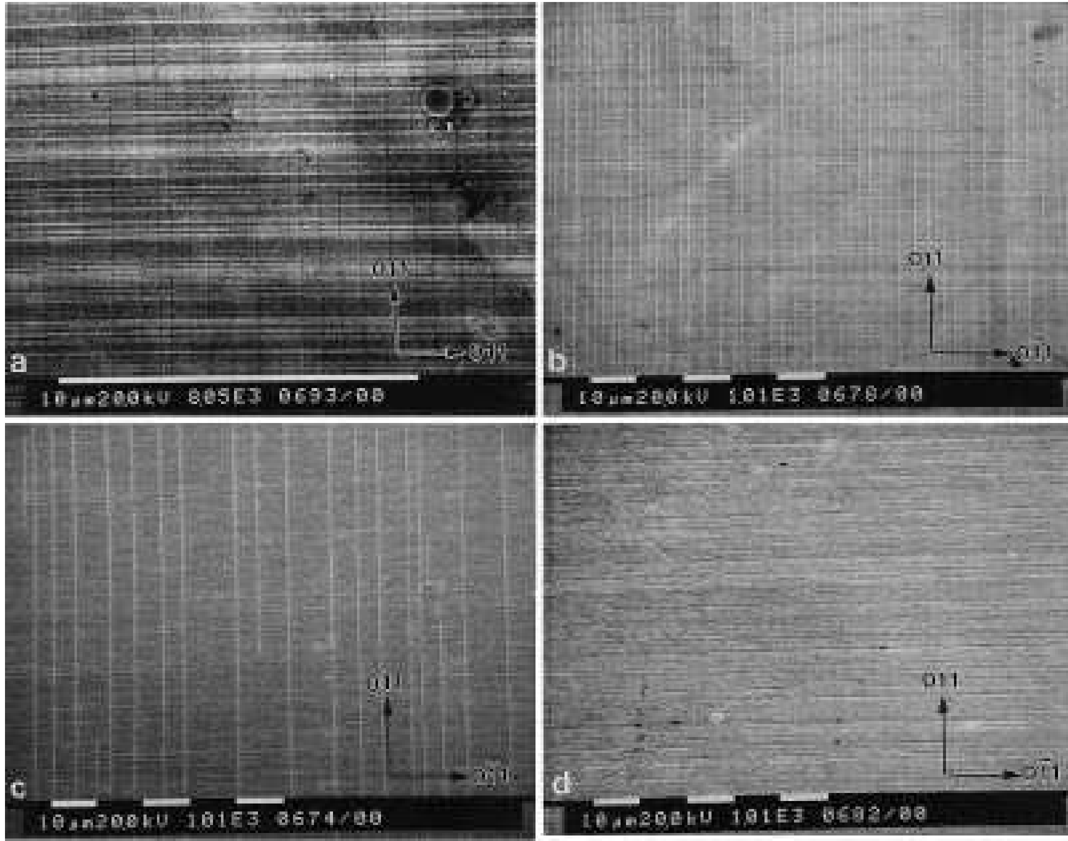

Fig. 4. SEM images of epilayer surface showing cracks and roughness contrast. The density of cracks decreases with an increase in layer thickness. No cracks were observed in the 500 nm thick layer: (a) $h = 20$ nm; (b) $h = 100$ nm; (c) $h = 200$ nm; (d) $h = 500$ nm.

4.1. Single crack behaviour

Prior to the introduction of any dislocations (twins), cracks or surface roughening, the epitaxial film is in a state of balanced biaxial tension, while the substrate is under compression. If we ignore wafer bending [this is a valid approximation here as the substrate thickness (h_s)$\gg$film thickness (h)], the stresses in the film and substrate are given by

$$\sigma^{f}_{yy} = \sigma^{f}_{zz} = 2\mu\frac{1+\nu}{1-\nu}f\cdot\frac{h_s}{h+h_s} \quad \text{(film)} \qquad \text{(1a)}$$

$$\sigma^{s}_{yy} = \sigma^{s}_{zz} = -2\mu\frac{1+\nu}{1-\nu}f\cdot\frac{h}{h+h_s} \quad \text{(substrate)} \qquad \text{(1b)}$$

where the x-, y- and z-axes are parallel to $[\bar{1}00]$, $[0\bar{1}1]$ and [011], respectively.

In these expressions, f is the misfit $\Delta a/a$ between the lattice parameters of $In_{0.25}Ga_{0.75}As$ and InP ($f = 0.02$ in this study), and identical elastic constants are assumed for the film and substrate. Two conditions have to be satisfied for crack nucleation. A necessary condition is that the stress at the surface of the film is at least equal to the (011) cleavage stress (σ_c). If $h_s \gg h$, and the surface remains planar, this condition can be written as

$$2\mu\frac{1+\nu}{1-\nu}f \geq \sigma_c.$$

In a surface roughened film this expression will underestimate the value of σ_c as the maximum stress will be highest at the valleys of the roughened surface. If this effect is ignored, a value of $\sigma_c \leq E/34$ is obtained by substituting E (Young's modulus) for $2\mu(1+\nu)$, 0.02 for f and 0.32 for ν.

A second and sufficient condition for crack formation, leading to the critical thickness concept, is that the energy of the system should be lowered by the introduction of a crack [13–17]. The analysis given by Thouless [13] and Thouless *et al.* [14] can be adapted to the plane stress situation described by equations (1a) and (1b), yielding a critical thickness given by

$$h_c = \frac{\Gamma_f(1-\nu)^2}{1.26\pi\mu(1+\nu)f^2} \qquad (2)$$

where Γ_f is the fracture resistance of the film. Substituting in values for μ and ν from Table 2, 0.02 for f, and knowing that h_c lies between 10 and

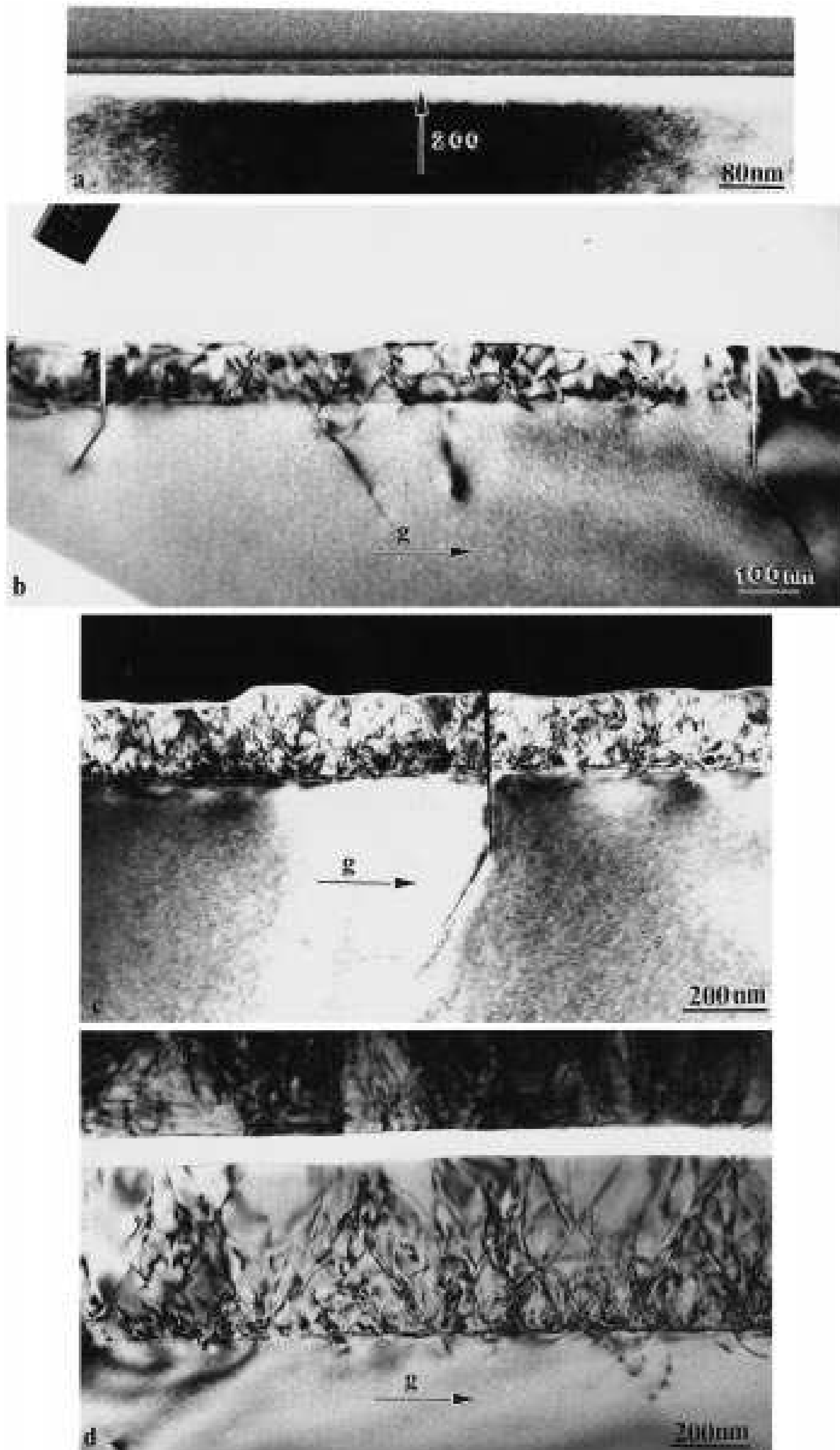

Fig. 5. The change of the structure with the change in layer thickness: (a) $h = 10$ nm, $\mathbf{g} = 200$; (b) $h = 100$ nm, $\mathbf{g} = 0\bar{2}2$; (c) $h = 200$ nm, $\mathbf{g} = 0\bar{2}2$; (d) $h = 500$ nm, $\mathbf{g} = 0\bar{2}2$. Note the increased dislocation activity seen in [011] cross-sections as the film thickness increases.

Table 1. Summary of measurements of crack dimensions with different layer thickness

Layer thickness, h (nm)	20	100	200
Crack spacing, d (nm) (SEM)	600 ± 190	2040 ± 580	4980 ± 1320
Crack spacing, d (nm) (TEM)	630 ± 230	2190 ± 470	4900 ± 1660
Crack length, c (nm) (TEM)	44 ± 1.2	300 ± 60	560 ± 80
Crack opening displacement, δ_0 (nm) (TEM)	5.8 ± 0.4	10 ± 0.7	15 ± 2.3

20 nm, we find that

$$1.32\ \mathrm{J/m^2} < \Gamma_f < 2.64\ \mathrm{J/m^2}.$$

For a purely elastic fracture $\Gamma_f = 2\gamma$: at room temperature 2γ is estimated to be $1.54\ \mathrm{J/m^2}$ for $In_{0.25}Ga_{0.75}As$ (Table 2). At the growth temperature (480°C), the surface energy will be slightly lower than this. Assuming a temperature dependence $\partial\gamma/\partial T = -0.1\ \mathrm{mJ/m^2\,(^\circ C)^{-1}}$ [20], $2\gamma = 1.45\ \mathrm{J/m^2}$ at the growth temperature. This value lies within the range for Γ_f found experimentally, suggesting that the initial fracture process is essentially elastic in nature. Neither of the Matthews and Klokholm [8] nor Murray *et al.* [10] values for h_c, discussed in Section 1 $[\Gamma_f(1-\nu)^2/(2\pi\mu(1+\nu)f^2)$ or $\Gamma_f(1-\nu)/(2\mu(1+\nu)f^2)$, respectively] gives as good agreement with the experimental data as does equation (2).

4.2. Multiple cracking and substrate cracking

The classical analyses of film cracking assume that arrays of parallel cracks spread across the film with little or no penetration of the crack into the substrate [13–17]. Cracks start to interact when the ratio of the crack spacing (d) to film thickness (h) is less than about 8 [13, 14], and an equilibrium spacing (<8 h) can be achieved by minimizing the total energy of the system, including the crack–crack interaction energy terms [14]. In our experiments, d/h lies between about 20 and 30, so crack interactions can be neglected. Nevertheless, a further reduction in energy can be achieved by allowing the crack to penetrate into the substrate. Although Ye *et al.* [17] state that crack penetration into the substrate is negligible when $\Gamma_s/\Gamma_f \approx 1$ (Γ_s is the fracture resistance of the substrate), our results suggest otherwise. The total strain energy (G) released by substrate cracking can be estimated from the stress-intensity factors given by Tada *et al.* [21]. The approach is described in the Appendix. For a crack of total length c, G is given by equations (A4) and (A5) in the Appendix, i.e.

$$G = \frac{1.98\sigma^2 c^2}{E}, \quad c \le h$$

$$G = \frac{1.98\sigma^2 h^2}{E} + \frac{4\sigma^2}{\pi E}\int_h^c x\left[\sin^{-1}\left(\frac{h}{x}\right)F\left(\frac{h}{x}\right)\right]^2 \mathrm{d}x, \quad c \ge h. \tag{3}$$

The total change in energy of the system is

$$\Delta E = -G + \Gamma_f c, \quad c \le h$$

$$\Delta E = -G + \Gamma_f h + \Gamma_h(c-h) = -G + \Gamma c, \text{ if } \Gamma_f = \Gamma_h = \Gamma, \quad c \ge h. \tag{4}$$

In order to compare the experimental observations with the predictions of equations (3) and (4), we should note that the stress in the film is progressively relaxed as growth proceeds by four competing processes: cracking, twinning, 60° dislocation formation and surface roughening. Since it is difficult to calculate the stress we have chosen to estimate σ from the experimental observations of c and δ_0 (the crack opening displacement) as a function of h (see Table 1). The method of calculation is indicated in Fig. 7(a), which shows ΔE plotted as a function of c/h for a film of thickness $h = 20$ nm at three stress values (1.8, 2 and 2.2 GPa). ΔE is initially positive but becomes negative at the critical thickness given by equation (2) with $\Gamma_f = 1.45\ \mathrm{J/m^2}$. The energy released passes through a minimum position before slowly rising to become zero again. It

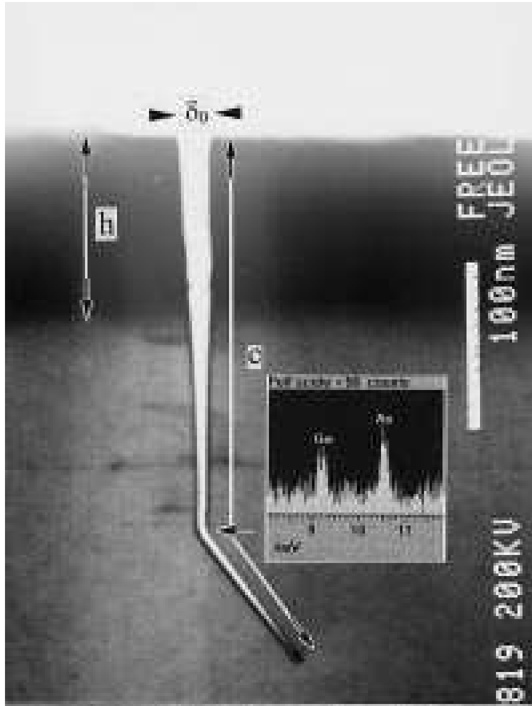

Fig. 6. STEM image of crack in 100 nm thick sample, showing the total crack length (c) and crack opening displacement (δ_0). The EDX spectrum from the crack region in the substrate of 100 nm thick sample, showing Ga and As signals.

Table 2. Properties of III–V compounds

	InP	GaAs	InAs	$In_{0.25}Ga_{0.75}As$
Shear modulus, μ (GPa)	22.3[a]	32.5[a]	19.0[a]	29.1
Poisson's ratio, ν	0.360[a]	0.312[a]	0.352[a]	0.322
Thermal expansion coefficient (10^{-6}/K)	4.5[b]	6.0[b]	5.2[b]	5.8
Surface energy, γ (J/m^2)				
{110}	0.75[c]	0.86[d]	0.57[c]	0.77
{111}	0.65[c]	0.75[c]	0.48[c]	0.68

[a] Adachi, S., *J. appl. Phys.*, 1982, **53**, 8775.
[b] Neuberger, M., *Handbook of Electronic Materials*, Vol. 2. IFI/Plenum, New York, 1972.
[c] Estimated values from Cahn, J. W. and Hanneman, R. E., *Surf. Sci.*, 1964, **1**, 387 (see text).
[d] Messmer, C. and Bilello, J. C., *J. appl. Phys.*, 1982, **52**, 4623.

seems reasonable to assume that the stable crack position in the substrate corresponds to this minimum. For the 20 nm thick film, $c/h \cong 2$ and a stress level of 2.2 GPa provides a good fit to the data. The stress in the uncracked film ($E/34$) is 2.26 GPa so this estimate appears plausible. The predicted value of δ_0 from equation (A2) in the Appendix, 5.4 nm, also compares favourably with the experimental measurement of 5.8 nm (see Table 1).

The same procedures were followed for the 100 and 200 nm thick films ($c/h = 3$ and 2.8, respectively). Stress levels of 1.2 GPa [Fig. 7(b)] and

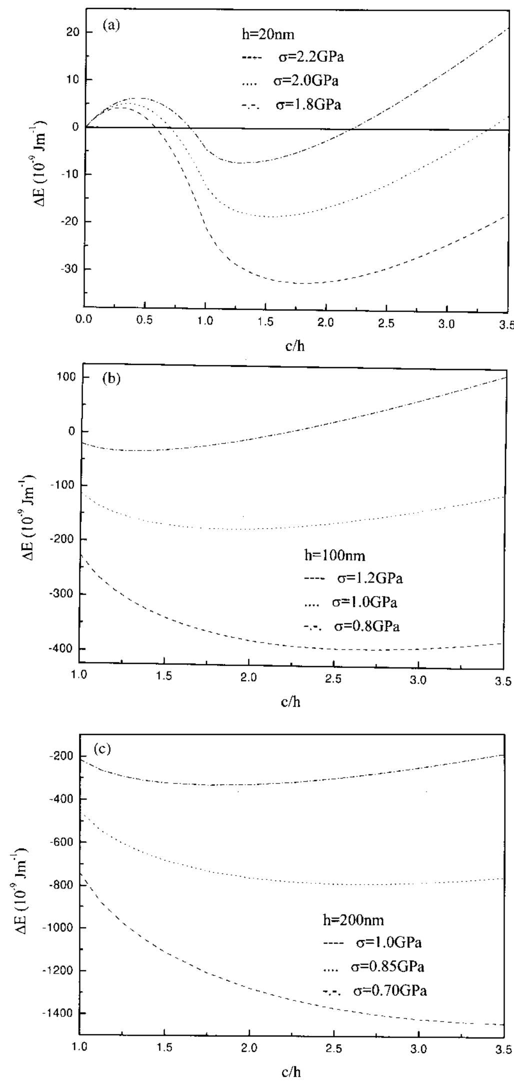

Fig. 7. Plots of ΔE [equation (4)] vs c/h at different stress levels for film thicknesses: (a) $h = 20$ nm; (b) $h = 100$ nm; (c) $h = 200$ nm.

0.85 GPa [Fig. 7(c)] were estimated for the effective stress acting in these films. Again these numbers appear reasonable, and point to the progressive relaxation of the film stress by plastic flow and surface roughening. The predicted crack opening displacements, 16 and 22 nm, respectively, are slightly greater than the average measured values, 10 and 15 nm. However, given the various assumptions made (isotropic elasticity, isotropic surface energies in the film and substrate and a uniform far field stress acting on each crack), the agreement is still satisfactory.

Two factors probably contribute to the deviation of the crack path from {110} to {111} in the substrate. The {111} surface energy of III–V compounds is about 13% lower than the {110} values (see Table 2). Secondly the "T-stress", that is the stress acting parallel to the crack when it penetrates into the substrate, can influence the crack path [16, 17].

4.3. Anisotropy of cracking

The InGaAs/InP system studied in this work represents an extreme case where stress relief in one of the two orthogonal ⟨011⟩ directions first occurs by twinning (Fig. 3), while in the other direction it occurs by cracking (Fig. 1). Similar observations have been reported by Olsen *et al.* [22] and Murray *et al.* [10]. The critical thickness for the nucleation of stacking faults or twins [23] in this system is very similar to the critical thickness for crack formation calculated above, equation (2). Given the approximate nature of these calculations, it is impossible to decide whether one mechanism would be favoured

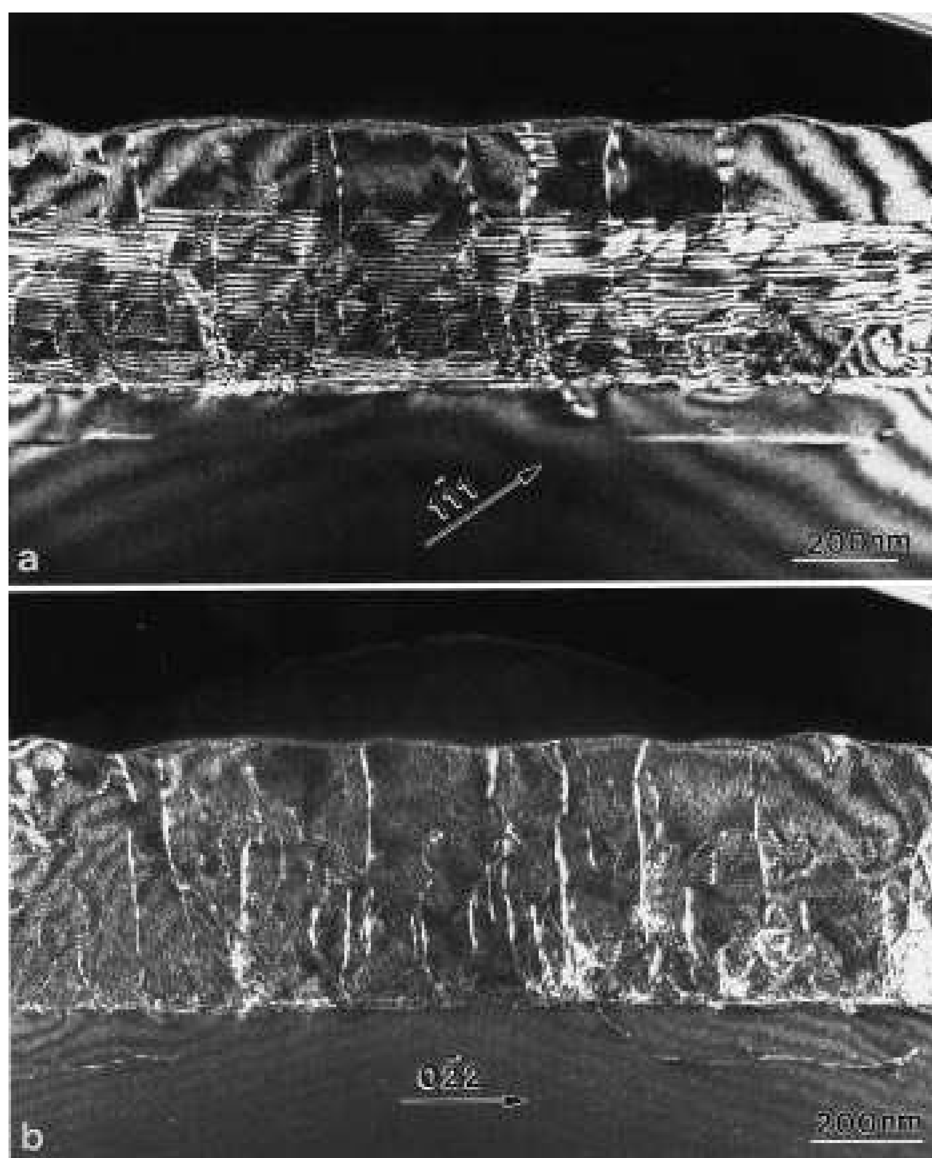

Fig. 8. Weak beam dark field images showing a high density of stacking faults and perfect dislocations in the 500 nm thick layer: (a) $\mathbf{g} = 1\bar{1}1$; (b) $\mathbf{g} = 0\bar{2}2$.

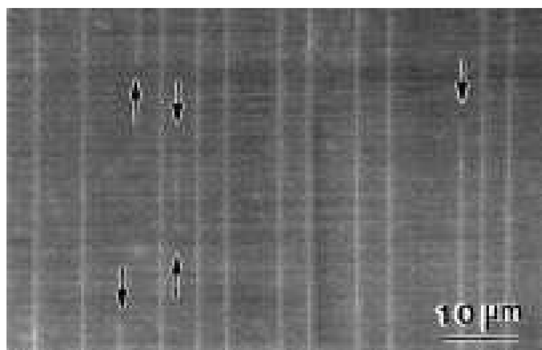

Fig. 9. SEM image of the surface of the 200 nm thick layer showing short cracks and crack terminations.

over another. The probable explanation for the observed asymmetry lies in the different nucleation characteristics of α and β dislocations [24, 25], and the role played by surface roughening in both stacking fault (twin) nucleation and cracking.

4.4. Crack healing

The single most intriguing observation of this study was the progressive drop in the density of cracks as film growth proceeds in the range from 20 to 200 nm, followed by the total elimination of cracks in the 500 nm thick film. These were such unexpected observations that a number of repeat growths and cross-checks were carried out to ensure that the results were reproducible and representative. The data presented in Table 1 demonstrate that a destructive sample preparation technique, cross-sectional transmission electron microscopy, and a non-destructive technique, scanning electron microscopy, give essentially identical crack densities at each thickness. Similar results (not presented here) were observed with atomic force microscopy. The cross-sectional work also showed that the cracks were not being "buried" during growth, as reported by Murray *et al.* [26].

The initial stage of stress relief in 20 nm thick film occurred by cracking along $(0\bar{1}1)$ planes, and by twinning on (111) and $(\bar{1}11)$ planes. As growth of the film continued, both perfect $(a/2)\langle 011\rangle$ dislocations and stacking faults bounded by $(a/6)\langle 112\rangle$ partial dislocations were observed in the [011] cross-sections (see Fig. 8). Strain relief by plastic flow becomes a competitive mechanism to crack formation in this direction. The details of this process are unclear, but it might be associated with the formation of the dislocations at the crack tips (Fig. 2), interacting and multiplying as growth proceeds. Whatever the origin of the dislocations seen in Fig. 8, they must reduce the residual elastic strain (and stress) acting on the cracks in the epilayer, as noted earlier.

The crack healing process itself is a discontinuous one, i.e. there is not a spontaneous healing at the crack front that simply reverses the interatomic bond breaking that must accompany crack formation. Instead the cracks appear to heal from the ends of the sample (or at discrete locations along the crack front). This is most obvious on comparing the crack morphology in the 20 nm thick film, where long continuous cracks are observed, with the 200 nm thick film where short crack segments or crack terminations are frequently observed (Fig. 9). Crack healing is probably driven by surface diffusion. As plastic flow starts to relieve the stresses acting on the cracks, the capillary stress at the crack tip ($\sim\gamma\kappa$, where γ is the surface energy and $\kappa = 1/\rho_1 + 1/\rho_2$ with ρ_i the principal radii of curvature) could become greater than the residual elastic stress. There would then be a driving force for surface diffusion of atoms to the crack tip and crack healing. The extreme purity of the atmosphere of the growth chamber in the molecular beam epitaxy process, and the constant supply of atoms from the surrounding atmosphere during growth would both aid crack healing.

Support for this hypothesis comes from energy dispersive X-ray analysis of the crack tips in TEM cross-sections. Figure 6 shows the X-ray spectrum from the crack tip region in the substrate at some distance from the epilayer. Both Ga and As were detected at this location in the 100 and 200 nm thick samples, but not in the 20 nm thick sample. These atoms could only come from the MBE growth atmosphere.

If crack healing turns out to be commonly found in the growth of III–V compounds, it highlights the pitfalls in relying solely on an energy criterion [8, 10, 13–17] to derive the critical film thickness for cracking. One might conclude from the observation of films whose thickness $\gg h_c$ that cracking had not occurred, whereas (as shown here) the films have first cracked and then the cracks have healed on further film growth.

5. CONCLUSIONS

1. Strain relief in epitaxial $In_{0.25}Ga_{0.75}As$ films (misfit = 2%) grown on (100) InP substrates is highly anisotropic. In the first stages of film growth, the strain was relieved by cracking on $(0\bar{1}1)$, while it occurred by (111) and $(\bar{1}11)$ twinning in the orthogonal direction.
2. Cracking was a transitory phenomenon. The 10 and 500 nm thick films were crack free, while a decreasing crack density was observed in the film thickness range from 20 to 200 nm.
3. The critical film thickness for cracking (~20 nm) corresponded to a condition where the total energy change (the sum of the elastic and surface energy) was zero.
4. Crack healing was observed in the 500 nm thick film. This was accompanied by increased dislo-

cation activity relieving the misfit along $[0\bar{1}1]$. Strain relief in this direction (by dislocation activity) must reduce the residual elastic stress acting on the $(0\bar{1}1)$ cracks, so that crack healing by surface diffusion of atoms to the sharp tip of the crack becomes a competitive process.

5. Cracks were observed to penetrate into the substrate and deviate from an $(0\bar{1}1)$ to $(1\bar{1}1)$ or $(\bar{1}\bar{1}1)$ planes. A critical stress intensity argument was developed to explain substrate cracking.

Acknowledgements—The authors are grateful to NSERC (Canada) for financial support, and to B. Robinson for growing the films.

REFERENCES

1. Frank, F. C. and van der Merwe, J. H., *Proc. R. Soc.*, 1949, **A198**, 216.
2. Matthews, J. W. and Blakeslee, A. E., *J. Cryst. Growth*, 1974, **27**, 118.
3. Dynna, M. and Weatherly, G. C., *J. Cryst. Growth*, 1994, **142**, 315.
4. Dunstan, D. J., *J. Mater. Sci.: Mater. Electron.*, 1997, **8**, 337.
5. Srolovitz, D. J., *Acta metall.*, 1989, **37**, 621.
6. Grilhe, J., *Acta metall. mater.*, 1993, **41**, 909.
7. Okada, T., Weatherly, G. C. and McComb, D. W., *J. appl. Phys.*, 1997, **81**, 2185.
8. Matthews, J. W. and Klokholm, E., *Mater. Res. Bull.*, 1972, **7**, 213.
9. Tsuchiya, T., Taniwatrai, T., Komori, M., Tsuneta, R. and Kakibayashi, H., *Japan. J. appl. Phys.*, 1994, **33**, 230.
10. Murray, R. T., Kiely, C. J. and Hopkinson, M., *Phil. Mag.*, 1996, **A74**, 383.
11. Dieguez, A., Vila, A., Cornet, A., Clark, S. A., Westwood, D. J. and Morante, J. R., *J. Vac. Sci. Technol.*, 1997, **A15**, 687.
12. Besser, P. J., Mee, J. E., Elkins, P. E. and Heinz, D. M., *Mater. Res. Bull.*, 1971, **6**, 1111.
13. Thouless, M. D., *J. Am. Ceram. Soc.*, 1990, **73**, 2144.
14. Thouless, M. D., Olsson, E. and Gupta, A., *Acta metall. mater.*, 1992, **40**, 1287.
15. Beuth, J. L., *Int. J. Solids Struct.*, 1992, **29**, 1657.
16. Hutchinson, J. W. and Suo, Z., *Adv. appl. Mech.*, 1991, **29**, 63.
17. Ye, T., Suo, Z. and Evans, A. G., *Int. J. Solids Struct.*, 1992, **29**, 2639.
18. Perovic, D. D., Weatherly, G. C. and Houghton, D. C., *Phil. Mag.*, 1991, **64A**, 1.
19. Dundurs, J., *J. appl. Mech.*, 1969, **36**, 650.
20. Tu, K.-N., Mayer, J. W. and Feldman, L. C., *Electronic Thin Film Science*. Macmillan, New York, 1992.
21. Tada, H., Paris, P. C. and Irwin, G. R., *The Stress Analysis of Cracks Handbook*. Del Research, St. Louis, MO, 1985.
22. Olsen, G. H., Abraham, M. S. and Zamerouski, T. J., *J. electrochem. Soc.*, 1974, **121**, 650.
23. Dynna, M. and Marty, A., *Acta mater.*, 1998, **46**, 1087.
24. DeCooman, B. C. and Carter, C. B., *Acta metall.*, 1989, **37**, 2765.
25. Kavanagh, K. L., Capano, M. A., Hobbs, L. W., Maree, P. M. J., Schaff, W., Mayer, J. W., Pettit, D., Woodall, J. M., Stroscio, J. A., Feenstra, R. M. and Barbour, J. C., *J. appl. Phys.*, 1988, **64**, 4843.
26. Murray, R. T., Hopkinson, M. and Kiely, C. J., *Inst. Phys. Conf. Ser.*, 1997, **153**, 425.

APPENDIX

Strain Energy Release Rate for Substrate Cracking

The geometry and stress intensity factors associated with a crack of total length c, subjected to a uniform normal stress σ acting along a segment of length h (corresponding to the epilayer stress) have been given by Tada *et al.* [21]. The crack opening displacement at the surface (δ_0) and the interface (δ_b), as well as the area of the crack (in the epilayer), are shown in Fig. A1. The stress intensity factor for this geometry is

$$K = \sigma\sqrt{\pi c}\cdot\frac{2}{\pi}\sin^{-1}\left(\frac{h}{c}\right)\cdot F\left(\frac{h}{c}\right). \quad \text{(A1)}$$

In this expression $\sigma\sqrt{\pi c}\cdot(2/\pi)\sin^{-1}(h/c)$ is the stress intensity factor for an internal crack in an infinite body, length $2c$, loaded in tension along a length $2h$, while $F(h/c)$ represents a surface correction term. Tada *et al.* [21] show that $F(h/c) \cong 1.3 - 0.18(h/c)$. δ_0 is given by

$$\delta_0 = \frac{4\sigma c}{E}\cdot\frac{2}{\pi}\left(\sin^{-1}\frac{h}{c}+\frac{h}{c}\cosh^{-1}\frac{c}{h}\right)H_0\left(\frac{h}{c}\right) \quad \text{with}$$

$$H_0\left(\frac{h}{c}\right) = 1.681 - 0.227\frac{h}{c}\left[1+\left(1-\frac{h}{c}\right)\left(\frac{h}{c}\right)^{-3/4}\right]. \quad \text{(A2)}$$

As the crack opens up, the work done by the stress, i.e. the reduction in elastic strain energy of the system, can be expressed as

$$G = -\frac{1}{2}\sigma\int_{\delta_b}^{\delta_0}\delta(x)\,dx \quad \text{(A3)}$$

where the integral is the shaded area in Fig. A1. This can be shown to be identical to the approach used by Ye *et al.* [17], where they divide G into two integrals, the first (G_1) accounting for the energy released as the crack penetrates through the epilayer, the second (G_2) as it passes into and arrests in the substrate.

G_1 and G_2 are given by

$$G_1 = \int_0^h \frac{K^2}{E}dx = \int_0^h \frac{\left(1.12\sigma\sqrt{\pi x}\right)^2}{E}dx = \frac{1.98\sigma^2h^2}{E} \quad \text{(A4)}$$

$$G_2 = \int_h^c \frac{K^2}{E}dx = \frac{4\sigma^2}{\pi E}\int_h^c x\left[\sin^{-1}\left(\frac{h}{x}\right)F\left(\frac{h}{x}\right)\right]^2 dx. \quad \text{(A5)}$$

The total energy released is $G_1 + G_2$ and the crack arrests when $(\partial/\partial c)(G - \Gamma_f c) = 0$.

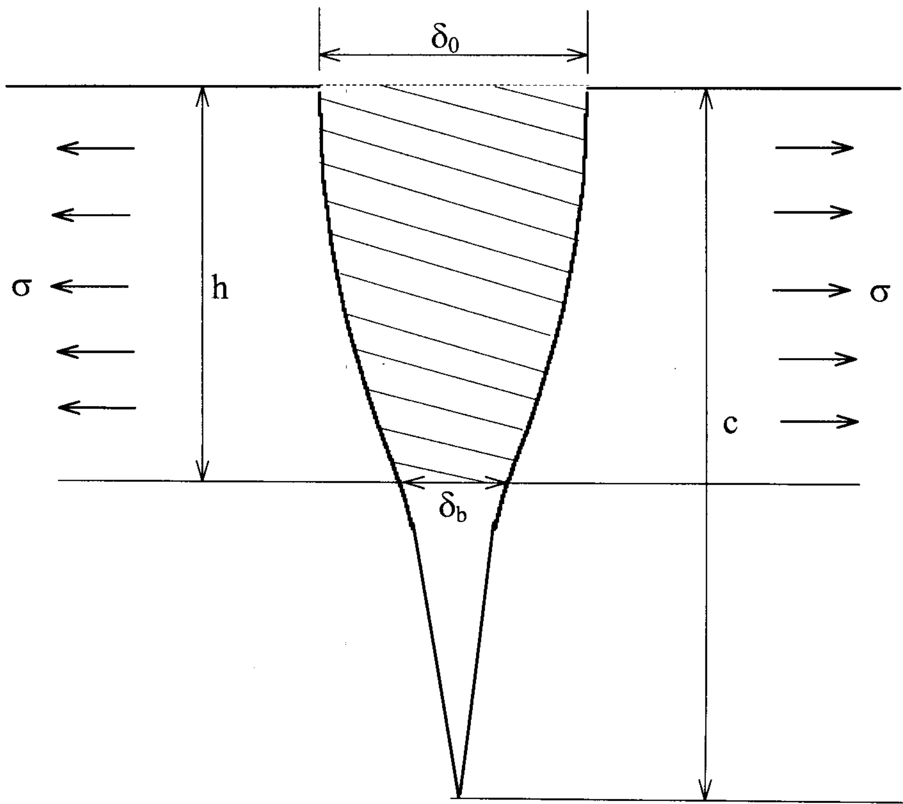

Fig. A1. Geometry of surface crack in epilayer (after Tada *et al.* [21]).